Letter

Entropic measure of directional emissions in microcavity lasers

Kyu-Won Park,[1] Chang-Hyun Ju,[2] and Kabgyun Jeong[1,3,*]

[1]*Research Institute of Mathematics, Seoul National University, Seoul 08826, Korea*

[2]*Department of Electronic Engineering, Yeungnam University, Gyeongsan 38541, Korea*

[3]*School of Computational Sciences, Korea Institute for Advanced Study, Seoul 02455, Korea*

(Received 31 May 2022; accepted 31 August 2022; published 15 September 2022)

We propose a notion of the directional emission in microcavity lasers. First, the Shannon entropy of the far-field profiles in the polar coordinate can quantify the degree of unidirectionality of the emission, while previous notions about the unidirectionality cannot efficiently measure in the robust range against a variation of the deformation parameter. Second, a divergence angle of the directional emission is defined phenomenologically in terms of full width at half maximum, and it is only easily applicable to a simple peak structure. However, the Shannon entropy of semimarginal probability of the far-field profiles in the Cartesian coordinate can present equivalent results, and moreover it is applicable even to cases with a complicated peak structure of the emission.

DOI: 10.1103/PhysRevA.106.L031504

Microcavity lasers have recently garnered considerable attention owing to their applicability as optimal candidate models for studying wave chaos [1,2] and non-Hermitian quantum systems [1,3,4] as well as their optoelectronic applications and photonics [5] such as speckle-free full-field imaging [6], and broadband coupling [7]. In addition, recent studies have revealed many interesting physics in phase space related to photon transport [8,9]. In particular, the key to such applications is that microcavity lasers have high-quality (Q) factors and directional emission simultaneously [10,11]. High-Q modes guarantee low threshold lasing; in addition, they can be adopted for biomolecule detections [12,13] and nanoparticles [14,15]. However, they are limited by isotopic emissions and low output power. Hence, directional emission is also required to support high output power, and also facilitate easy coupling to a waveguide for optoelectronic circuits. Therefore, to date, several microcavity lasers have been studied to achieve these properties simultaneously [16–21].

In these studies, the discussions about a high Q-factor have been addressed quantitatively and systemically, because the Q factor can be well defined by $Q = \frac{f_r}{\Delta f}$, where f_r is a resonance frequency and Δf is a resonance width, or equivalently, $Q = \frac{f_r}{2|f_i|}$ in the context of a complex eigenfrequency $f_c = f_r + jf_i$. However, regarding directional emission, we consider that its definition is relatively subtle and it remains not well established up to date. In this Letter, thus, we introduce measures of the unidirectional emission by exploiting the notion of Shannon entropy, and this suggestion holds that an entropic measure of the unidirectional emission is more accurate and efficient than former alternatives related to the emission window [22,23]. It is possible to validate these results by demonstrating that former alternatives fail to detect the degree of the directional emission, yet our methods can.

To further engage this discussion, we consider a prevalent and basic limaçon-shaped microcavity laser as a candidate for the directional emission with a high Q factor [10,11,24,25], as it has been extensively studied to date. The geometrical boundary of the limaçon-shaped microcavity is defined as follows,

$$R(\theta) = R_0(1 + \chi \cos\theta), \tag{1}$$

where θ is the angle in the polar coordinate, χ is the deformation parameter, and $R_0(= 1)$ is the radius of circles at $\chi = 0$. The limaçon-shaped microcavity laser with an effective index of refraction $n = 3.3$ (for an InGaAsP semiconductor microcavity) is treated in a ray simulation. Some of the representative far-field profiles (FFPs) in the limaçon-shaped cavity are shown in Fig. 1. The FFPs are obtained from transmitted rays by using Fresnel equations for transverse magnetic (TM) modes. Figures 1(a)–1(c) are plotted in the Cartesian coordinate within the range of $|x| \leqslant 5$ and $|y| \leqslant 5$ at each deformation $\chi = 0.43$, $\chi = 0.454$, and $\chi = 0.478$, respectively. Figures 1(d)–1(f) are FFPs plotted in the polar coordinate, corresponding to FFPs in the Cartesian coordinate, respectively. We call the angles in the range of $|\theta| \leqslant \frac{\pi}{4}$ as the "emission window," which was first introduced by Refs. [22,23] for the definition of unidirectionality.

It was reported that the deformation parameter $\chi = 0.43$ is the optimal value for unidirectional emission [10]. Moreover, they have concluded that the results are robust against any variation of the deformation parameter in the range of $0.43 \leqslant \chi \leqslant 0.49$ [10]. Consistent with their results, the overall profiles of Fig. 1 appear similar to each other. However, if we observe the morphologies of FFPs for Figs. 1(d)–1(f) simultaneously, we can suggest that FFPs at $\chi = 0.454$ exhibit a larger unidirectionality than the others.

To validate this suggestion, we address three types of measure for the unidirectionality. The blue squares (U_W) and red circles (U_C) in Fig. 2(a) are measures of the unidirectionality associated with the emission windows. More precisely, the

*kgjeong6@snu.ac.kr

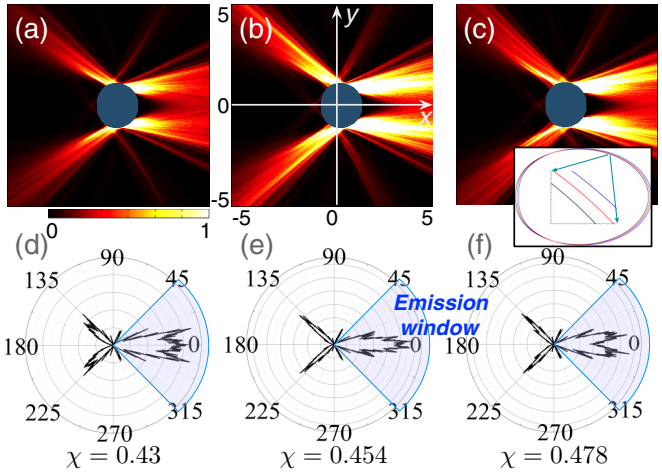

FIG. 1. Far-field profiles in a limaçon-shaped cavity. (a)–(c) are the far-field profiles in the Cartesian coordinate within $x \in [-5, 5]$ and $y \in [-5, 5]$ at each deformation $\chi = 0.43$, $\chi = 0.454$, and $\chi = 0.478$, respectively. (d)–(f) are also far-field profiles plotted in the polar coordinate corresponding to the far-field profiles in the Cartesian coordinate. The angles in the range of $|\theta| \leqslant \frac{\pi}{4}$ are the emission window. The inset in (c) shows the boundary shape of the cavity at each $\chi = 0.43$ (black lower line), 0.454 (red center line), and 0.478 (blue upper line), respectively.

unidirectionality U_C marked by red circles is defined as follows [26,27]:

$$U_C = \frac{\int_0^{2\pi} I(\theta)\cos\theta d\theta}{\int_0^{2\pi} I(\theta) d\theta}. \tag{2}$$

Here, $I(\theta)$ denotes the intensity of angular distribution of FFPs [28]. The $\cos\theta$ as a window function determines the extent to which the emission directionality deviates from unidirectionality. Actually, the positive and negative U_C represent tendencies toward a forward and backward emission, respectively, and $U_C = 0$ corresponds to the bidirectional or isotropic emission of the microcavity laser. In our case, the values of U_C almost increase linearly from $U_C \simeq 0.3$ to $U_C \simeq 0.35$ in the range of $0.43 \leqslant \chi \leqslant 0.478$. This result implies that the unidirectionality increases as the deformation parameter χ increases, unlike observing the morphologies of FFPs

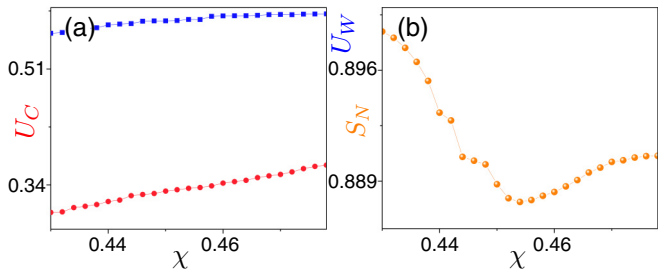

FIG. 2. Three types of measure of unidirectionality in the limaçon-shaped cavity. The blue squares (U_W) and red circles (U_C) in (a) are measures of unidirectionality associated with the emission window. They almost increase linearly as a function of the deformation. The orange circles in (b) are normalized Shannon entropies and they have a local minimum at $\chi = 0.454$.

for Figs. 1(d)–1(f). Note that we here discretize 2π into 3600 pieces for numerical calculation, i.e., $d\theta \sim \Delta\theta = 0.1^\circ$.

The other measure of the unidirectionality U_W marked by blue squares is also defined as follows [22,23],

$$U_W = \frac{\int_{\frac{-\pi}{4}}^{\frac{\pi}{4}} I(\theta) d\theta}{\int_0^{2\pi} I(\theta) d\theta}, \tag{3}$$

where the integral range of the numerator runs from $-\frac{\pi}{4}$ to $\frac{\pi}{4}$. The angles in this range of $|\theta| \leqslant \frac{\pi}{4}$ are the so-called emission window as mentioned before.

Hence, the meaning of this definition is clearly the ratio between accumulated intensities of FFPs within the emission window and the total intensity of FFPs. The values of U_W also increase almost linearly from $U_W \simeq 0.56$ to $U_W \simeq 0.59$ in the range of $0.43 \leqslant \chi \leqslant 0.478$. Consequently, these values of U_W are also inconsistent with our observation. We can conjecture that this discrepancy is attributed to the fact that U_W increases proportionally to the integral value of the emission window, regardless of the detailed structure of the emission window. Furthermore, it should be noticed that U_C exhibits a similar trend with U_W.

Next, we introduce entropic unidirectionality. Accordingly, we first have to obtain a Shannon entropy associated with FFPs. Shannon entropy is a relevant measure of the average amount of information for a random variable with a given probability distribution function [29]. It was first developed and utilized in communication theory [29]. However, recently it has been also exploited in various areas such as biosystems [30], economics [31], atomic physics [32], and microcavity lasers [33].

The discrete Shannon entropy for the intensity of FFPs is formally defined as

$$S_N = -\frac{1}{\ln K} \sum_{i=1}^{K} \rho_i \ln \rho_i, \tag{4}$$

where ρ_i represents the probability distribution obtained under the normalization condition $\sum_{i=1}^{K} I(\theta_i) = 1$. That is, the random variable X is an angular coordinate (Θ) with the probability distribution $\{\rho_i\} = \{P(\Theta = \theta_i)\}$. In addition, the $\frac{1}{\ln K}$ is a normalization factor such that the value of Shannon entropy is restricted in the range of $0 \leqslant S_N \leqslant 1$, with $K = 3600$ as mentioned above. The orange circles in Fig. 2(b) represent normalized Shannon entropy (S_N) calculated by this definition. The value of S_N has a local maximum (0.898) at $\chi = 0.43$ and local minimum (0.888) at $\chi = 0.454$, respectively.

Our recent works have confirmed that Shannon entropy can be beneficial in measuring the delocalization of the given probability distributions [34]. Hence, the minimum (or maximum) value of the Shannon entropy indicates the maximum localization (or delocalization) of the intensity of FFPs in the polar coordinate under the normalization condition $\sum_{i=1}^{K} I(\theta_i) = 1$. Consequently, the local minimum value of S_N at $\chi = 0.454$ directly verifies the maximal undirectionality. Moreover, the maximal entropy $\ln K$ corresponds to the isotropic distribution that is not a bidirectional emission in the polar coordinate. This result validates the conjecture that by

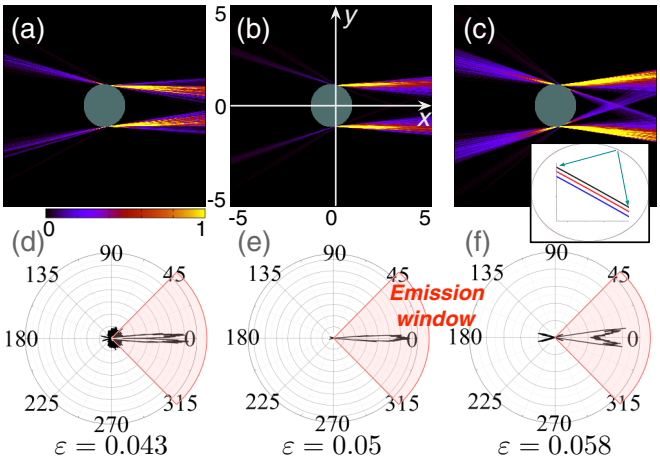

FIG. 3. FFPs in an oval-shaped microcavity laser. (a)–(c) are FFPs in the Cartesian coordinate restricted in the range of $x \in [-5, 5]$ and $y \in [-5, 5]$ at each deformation $\varepsilon = 0.043$, $\varepsilon = 0.05$, and $\varepsilon = 0.058$, respectively. (d)–(f) are also FFPs plotted in the polar coordinate corresponding to FFPs in the Cartesian coordinate. The inset in (c) shows the boundary shape of cavity at each $\varepsilon = 0.043$ (black upper line), 0.05 (red center line), and 0.058 (blue lower line), respectively

exploiting the Shannon entropy, our measure of unidirectionality is coincident with our observations in Fig. 1.

For more generality of our argument and to understand the discrepancy between Figs. 2(a) and 2(b), let us consider an oval-shaped microcavity laser [35]. The FFPs are also obtained from transmitted rays by using Fresnel equations for transverse electric (TE) modes with an effective index of refraction $n = 3.3$. The geometrical boundary condition of an oval-shaped cavity, which is deformed from an ellipse, is defined as follows:

$$\frac{x^2}{a^2} + (1 + \varepsilon x)\frac{y^2}{b^2} = 1. \tag{5}$$

For convenience, we substitute the deformation parameter χ to ε. It was reported that the optimized condition for a directional emission is $a = 1.0$, $b = 1.03$, and $\varepsilon = 0.05$, where a and b are the major and minor axis of an ellipse, and ε is the deformation parameter, respectively [35]. According to their results, we conduct a ray simulation in the range of $0.043 \leqslant \varepsilon \leqslant 0.058$ at fixed values of $a = 1.0$ and $b = 1.03$. We plot some of the representative FFPs, i.e., Figs. 3(a)–3(c) in the Cartesian coordinate restricted in $x \in [-5, 5]$ and $y \in [-5, 5]$ at each deformation $\varepsilon = 0.043$, $\varepsilon = 0.05$, and $\varepsilon = 0.058$. The corresponding FFPs in the polar coordinate are displayed in Figs. 3(d)–3(f).

In contrast to Fig. 1, we can easily notice that the overall FFPs depending on the deformation parameter vary manifestly, and it can be naturally expected that the local maximum of the unidirectionality is obtained at $\varepsilon = 0.05$ by observing Figs. 3(b) and 3(e), and comparing other subpanels in Fig. 3. In this case, the local minimum value of S_N, and local maximum values of U_W and U_C are attained at $\varepsilon = 0.05$ simultaneously, i.e., the entropic measure of the unidirectionality S_N agrees well with the former measure of the unidirectionality (U_C, U_W) related to the emission window. Consequently, this

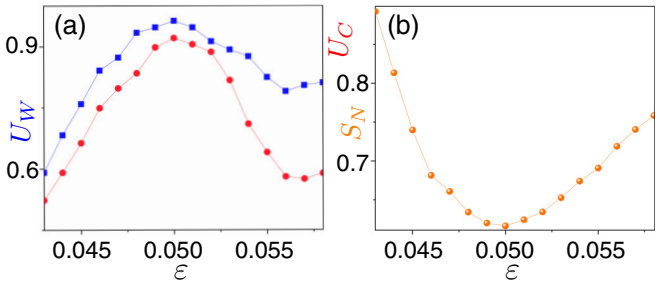

FIG. 4. Three types of measure of the unidirectionality in the oval-shaped microcavity. The blue squares and red circles in (a) are measures of the unidirectionality associated with the emission window. Both of them have local maximal values at $\varepsilon = 0.05$. The orange circles in (b) are normalized Shannon entropies. The values of orange circles have a local minimum value at $\varepsilon = 0.05$.

fact implies that U_C and U_W can only detect the unidirectionality when the overall FFPs vary significantly with a manifest variation of the emission window. However, our measure for the unidirectionality by employing the Shannon entropy can efficiently capture the unidirectionality in any case. Notice that the relative difference between the local maximum and the local minimum of S_N in Fig. 4 is much larger than that of Fig. 2. This fact coincides with our initial intuition.

Another aspect for the definition of the directional emission along with the unidirectionality is a so-called "divergence angle." This concept presents an analogy for the full width at half maximum (FWHM) [11]. In our case, the divergence angle estimates the width of the peak emission (i.e., the lobe around $\theta = 0$) [11,16] of the emission intensity in the polar coordinate, and this can indicate the degree of the spread of FFPs onto the y axis in the Cartesian coordinate. Under these assumptions, we first introduce the concept of semimarginal probability distribution. When the joint probability distribution function of random variables X and Y is given by $\rho(x, y)$, the marginal probability distribution of Y is $\rho(y) = \int \rho(x, y)dx$, where the integral is carried out over all points in the range of (X, Y) for which $Y = y$. We can interpret the intensity of FFPs, $I(x, y)$, in the Cartesian coordinate as a joint probability distribution function under the normalization condition $\iint I(x, y)dxdy = 1$, i.e., the random variables X and Y are components of the Cartesian coordinate with the joint probability distribution function $\rho(x, y) = P(X = x, Y = y)$. The integral $\int \rho(x, y)dx$ is performed over the interval $x \in [0, 5]$ to solely handle the forward emission. This is why we call it a semimarginal probability distribution. Note that we have discretized the (x, y) coordinate in the range $x \in [-5, 5]$ and $y \in [-5, 5]$ into a 1000×1000 grid for the numerical calculation. Then, the discrete Shannon entropy from $\rho(y_j)$ is defined by

$$S_y = -\frac{1}{\ln K}\sum_{j=1}^{K} \rho_{y_j} \ln \rho_{y_j}, \tag{6}$$

where the semimarginal distribution $\rho_{y_j} = \sum_{i=1}^{K} \rho(x_i, y_j)$ and $K = 1000$.

The blue squares in Fig. 5(a) represent the divergence angle (D_A) and the red spheres in Fig. 5(a) represent the Shannon

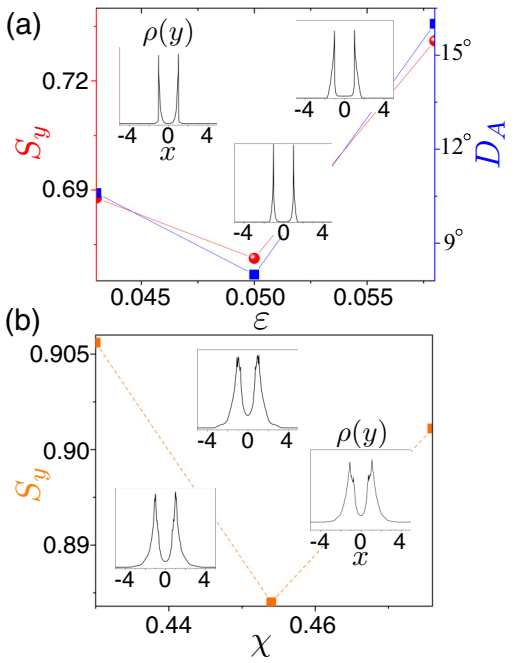

FIG. 5. (a) The blue squares are markers of the divergence angle (D_A) and the red circles are those of Shannon entropy of the semimarginal probability densities (S_y) in the oval-shaped microcavity laser at each $\varepsilon = 0.043$, $\varepsilon = 0.05$, and $\varepsilon = 0.058$. These two plots show similar trends. The three insets are semimarginal probabilities related to S_y. (b) The orange squares are markers of Shannon entropy of semimarginal probabilities (S_y) in the limaçon-shaped microcavity laser at $\chi = 0.43$, $\chi = 0.454$, and $\chi = 0.478$. The three insets are also semimarginal probabilities related to S_y.

entropy (S_y) of the semimarginal probabilities in the oval-shaped microcavity laser at each $\varepsilon = 0.043$, $\varepsilon = 0.05$, and $\varepsilon = 0.058$. Note that these two plots show similar trends and these results support our previous assumption. The three insets in Fig. 5 represent semimarginal probability densities (ρ_y). All peaks of ρ_y are located at $\varepsilon \simeq \pm 1$, and careful examination reveals that the third one is more spread out than the others.

In the case of complex peak structures, as illustrated in Figs. 1(d)–1(f), we can barely define D_A (i.e., FWHM). However, we can quantitatively and systematically measure the spread of the emission peak by exploiting S_y, and the obtained results are presented in Fig. 5(b). The orange squares in Fig. 5(b) indicate Shannon entropy (S_y) of semimarginal probability (ρ_y) in the limaçon-shaped cavity at $\chi = 0.43$, $\chi = 0.454$, and $\chi = 0.478$. The minimum value of S_y in Fig. 5(b) is substantially larger than that of S_y in Fig. 5(a), which can be confirmed by comparison between Figs. 1(e) and 3(e).

Consequently, we can say that the oval-shaped microcavity laser has larger unidirectionality and smaller S_y (i.e., D_A) than the limaçon-shaped microcavity laser at least in our examples. In contrast, the limaçon-shaped microcavity laser has a more robust range against any variation of the deformation parameter than the oval-shaped microcavity laser.

We have presented measures for directional emission in microcavity lasers by exploiting the Shannon entropy. There are primarily two aspects of the directional emission—the unidirectionality and the divergence angle. Shannon entropy obtained from the normalized intensity of angular distributions of FFPs can measure the unidirectionality even if former notions cannot effectively detect the directional emission when the emission is robust against a variation of the deformation parameter. However, it should be noticed that our method can be wrong in some extreme cases. For example, extreme bidirectional emission can yield a very low value of the Shannon entropy. In order to exclude such cases, each FFP must have a single broad but dominant emission. To guarantee this condition, an overlap between FFPs and Gaussian normal distribution must be larger than a critical value as the role of auxiliary measure. In the proposed examples, the overlaps are always larger than 0.6 with a mean value $\langle\theta\rangle = 0$ (corresponding to the emission peak) and standard deviation $\sigma = 45^\circ$ (corresponding to the emission window). Shannon entropy obtained from the semimarginal probability densities of FFPs in the Cartesian coordinates can provide equivalent results to the divergence angle; moreover, it can be applied even in the case of complicated peak structures.

Our measure is entirely defined by normalized FFPs (as probability distributions), regardless of the origin of emissions. Thus, our measure is applicable to the FFPs obtained from the wave simulations and, furthermore, it can be applicable to any shape of microcavity lasers and various antenna structures. We hope that our results can help to design and to modulate micocavity lasers for better directional emissions.

This work was supported by the National Research Foundation of Korea, a grant funded by the Ministry of Education (Grants No. NRF-2021R1I1A1A01052331 and No. NRF-2021R1I1A1A01042199) and the Ministry of Science and ICT (Grant No. NRF-2020M3E4A1077861).

[1] H. Cao and J. Wiersig, Dielectric microcavities: Model systems for wave chaos and non-Hermitian physics, Rev. Mod. Phys. **87**, 61 (2015).

[2] S. Liu, J. Wiersig, W. Sun, Y. Fan, L. Ge, J. Yang, S. Xiao, Q. Song, and H. Cao, Chaotic-to-regular tunneling: Transporting the optical chirality through the dynamical barriers in optical microcavities, Laser Photonics Rev. **12**, 1870045 (2018).

[3] K. Takata, N. Roberts, A. Shinya, and M. Notomi, Imaginary couplings in non-Hermitian coupled-mode theory: Effects on exceptional points of optical resonators, Phys. Rev. A **105**, 013523 (2022).

[4] K.-W. Park, J. Kim, S. Moon, and K. An, Maximal Shannon entropy in the vicinity of an exceptional point in an open microcavity, Sci. Rep. **10**, 12551 (2020).

[5] K. J. Vahala, Optical microcavities, Nature (London) **424**, 839 (2003).

[6] B. Redding, A. Cerjan, X. Huang, and H. Cao, Low spatial coherence electrically pumped semiconductor laser for

speckle-free full-field imaging, Proc. Natl. Acad. Sci. USA **112**, 1304 (2015).

[7] X. Jiang, L. Shao, S.-X. Zhang, X. Yi, J. Wiersig, L. Wang, Q. Gong, M. Lončar, L. Yang, and Y.-F. Xiao, Chaos-assisted broadband momentum transformation in optical microresonators, Science **358**, 344 (2017).

[8] L.-K. Chen, Y.-Z. Gu, Q.-T. Cao, Q. Gong, J. Wiersig, and Y.-F. Xiao, Regular-Orbit-Engineered Chaotic Photon Transport in Mixed Phase Space, Phys. Rev. Lett. **123**, 173903 (2019).

[9] Y.-J. Qian, H. Liu, Q.-T. Cao, J. Kullig, K. Rong, C.-W. Qiu, J. Wiersig, Q. Gong, J. Chen, and Y.-F. Xiao, Regulated Photon Transport in Chaotic Microcavities by Tailoring Phase Space, Phys. Rev. Lett. **127**, 273902 (2021).

[10] J. Wiersig and M. Hentschel, Combining Directional Light Output and Ultralow Loss in Deformed Microdisks, Phys. Rev. Lett. **100**, 033901 (2008).

[11] C. Yan, Q. J. Wang, L. Diehl, M. Hentschel, J. Wiersig, N. Yu, C. Pflügl, F. Capasso, M. A. Belkin, T. Edamura, M. Yamanishi, and H. Kan, Directional emission and universal far-field behavior from semiconductor lasers with limaçon-shaped microcavity, Appl. Phys. Lett. **94**, 251101 (2009).

[12] A. M. Armani, R. P. Kulkarni, S. E. Fraser, R. C. Flagan, and K. J. Vahala, Label-free, single-molecule detection with optical microcavities, Science **317**, 783 (2007).

[13] F. Vollmer and S. Arnold, Whispering-gallery-mode biosensing: label-free detection down to single molecules, Nat. Methods **5**, 591 (2008).

[14] J. Zhu, S. K. Ozdemir, Y.-F. Xiao, L. Li, L. He, D.-R. Chen, and L. Yang, On-chip single nanoparticle detection and sizing by mode splitting in an ultrahigh-Q microresonator, Nat. Photonics **4**, 46 (2010).

[15] W. Chen, Ş. Kaya Özdemir, G. Zhao, J. Wiersig, and L. Yang, Exceptional points enhance sensing in an optical microcavity, Nature (London) **548**, 192 (2017).

[16] Q. Jie Wang, C. Yan, L. Diehl, M. Hentschel, J. Wiersig, N. Yu, C. Pflügl, M. A. Belkin, T. Edamura, M. Yamanishi, H. Kan, and F. Capasso, Deformed microcavity quantum cascade lasers with directional emission, New J. Phys. **11**, 125018 (2009).

[17] Y.-D. Yang and Y.-Z. Huang, Mode characteristics and directional emission for square microcavity lasers, J. Phys. D: Appl. Phys. **49**, 253001 (2016).

[18] Q. Song and H. Cao, Highly directional output from long-lived resonances in optical microcavity, Opt. Lett. **36**, 103 (2011).

[19] J. Peter, M. Kailasnath, V. R. Anand, C. P. G. Vallabhan, and A. Mujeeb, Control of directional emission of resonance modes in an asymmetric cylindrical microcavity, Opt. Laser Technol. **105**, 1 (2018).

[20] L. Wang, C. Wang, J. Wang, F. Bo, M. Zhang, Q. Gong, M. Lončar, and Y.-F. Xiao, High-Q chaotic lithium niobate microdisk cavity, Opt. Lett. **43**, 2917 (2018).

[21] Y. Yang, J. Wang, L. Zhu, W. Chen, G. Wu, H. Wang, Y. Jia, Y. Huang, X. Ren, S. Luo, and H. Ji, Design optimization of silicon-based 1.55 μm InAs/InGaAs quantum dot square microcavity lasers with output waveguides, Laser Phys. **31**, 065803 (2021).

[22] J.-W. Ryu and M. Hentschel, Designing coupled microcavity lasers for high-Q modes with unidirectional light emission, Opt. Lett. **36**, 1116 (2011).

[23] J.-W. Ryu, J. Cho, I. Kim, and M. Choi, Optimization of conformal whispering gallery modes in limaçon-shaped transformation cavities, Sci. Rep. **9**, 1 (2019).

[24] S. Shinohara, M. Hentschel, J. Wiersig, T. Sasaki, and T. Harayama, Ray-wave correspondence in limaçon-shaped semiconductor microcavities, Phys. Rev. A **80**, 031801(R) (2009).

[25] Q. Song, W. Fang, B. Liu, S.-T. Ho, G. S. Solomon, and H. Cao, Chaotic microcavity laser with high quality factor and unidirectional output, Phys. Rev. A **80**, 041807(R) (2009).

[26] J.-B. Shim, A. Eberspächer, and J. Wiersig, Adiabatic formation of high-Q modes by suppression of chaotic diffusion in deformed microdiscs, New J. Phys. **15**, 113058 (2013).

[27] Q. Song, L. Ge, A. D. Stone, H. Cao, J. Wiersig, J.-B. Shim, J. Unterhinninghofen, W. Fang, and G. S. Solomon, Directional Laser Emission from a Wavelength-Scale Chaotic Microcavity, Phys. Rev. Lett. **105**, 103902 (2010).

[28] X.-F. Jiang, C.-L. Zou, L. Wang, Q. Gong, and Y.-F. Xiao, Whispering-gallery microcavities with unidirectional laser emission, Laser Photonics Rev. **10**, 40 (2016).

[29] C. E. Shannon, A mathematical theory of communication, Bell Syst. Tech. J. **27**, 379 (1948).

[30] S. Fuhrman, M. J. Cunningham, X. Wen, G. Zweiger, J. J. Seilhamer, and R. Somogyi, The application of Shannon entropy in the identification of putative drug targets, Biosystems **55**, 5 (2000).

[31] N. Eagle, M. Macy, and R. Claxton, Network diversity and economic development, Science **328**, 1029 (2010).

[32] R. González-Férez and J. S. Dehesa, Shannon Entropy as an Indicator of Atomic Avoided Crossings in Strong Parallel Magnetic and Electric Fields, Phys. Rev. Lett. **91**, 113001 (2003).

[33] K.-W. Park, S. Moon, Y. Shin, J. Kim, K. Jeong, and K. An, Shannon entropy and avoided crossings in closed and open quantum billiards, Phys. Rev. E **97**, 062205 (2018).

[34] K.-W. Park, J. Kim, J. Seo, S. Moon, and K. Jeong, Indicators of wavefunction (de)localisation for avoided crossing in a quadrupole quantum billiard, J. Phys. Commun. **5**, 115009 (2021).

[35] J.-W. Lee, C.-H. Yi, I.-G. Lee, J.-H. Kim, H.-H. Yu, K.-R. Oh, and C.-M. Kim, Extremely high Q and unidirectional laser emission due to combination of the Kolmogorov–Arnold–Moser barrier and the chaotic sea in a dielectric microdisk, Opt. Lett. **43**, 6097 (2018).